Experimental Eye Research 99 (2012) 98–104

Contents lists available at SciVerse ScienceDirect

Experimental Eye Research

journal homepage: www.elsevier.com/locate/yexer

Ultrasound imaging velocimetry of the human vitreous

Tommaso Rossi [a,*], Giorgio Querzoli [d], Giacomo Pasqualitto [c], Mario Iossa [a], Luca Placentino [a], Rodolfo Repetto [b], Alessandro Stocchino [b], Guido Ripandelli [e]

[a] Ospedale Oftalmico di Roma, Rome, Italy
[b] University of Genoa, DICAT, Italy
[c] Optikon 2000 Inc., Italy
[d] University of Cagliari, DIT, Italy
[e] Fondazione G.B. Bietti, IRCCS, Italy

ARTICLE INFO

Article history:
Received 18 January 2012
Accepted in revised form 27 March 2012
Available online 12 April 2012

Keywords:
Ultrasound Image Velocimetry
speckle tracking
ultrasound of the eye
human vitreous motion
retinal detachment

ABSTRACT

Knowledge of vitreous motion in response to saccades is a prerequisite for understanding vitreous rheology. Purpose of present paper is to introduce Ultrasound Image Velocimetry of the human eye, measure scleral and vitreous velocity fields and test the reproducibility of the proposed technique. Twelve patients with varying diagnosis underwent Ocular Dynamic Ultrasound; scleral angular velocity (V_S) was measured by 2 different operators and reproducibility calculated. Squared velocity of the vitreous (E), which is representative of kinetic energy per unit mass, was computed from velocity. The time evolution of the energy of the vitreous was described by its spatial average (E_S), whereas spatial distribution was described by its time average (E_T). Peak and average E_S, the ratio K_p of the peak of the spatially averaged kinetic energy per unit mass to the maximum squared scleral angular velocity, vitreous motion onset time (T_O) and vitreous motion decay time (T_D) were also defined. Inter-operator reproducibility coefficient was 0.043 and correlation between operators was significant. V_S, peak and average E_S, K_p ratio and T_D differed among patients but not among operators. V_S correlated with E_S and T_D. E_S and T_D but not V_S, were significantly different in patients with Posterior Vitreous Detachment. Patients with retinal detachment showed significantly higher V_S and E_S. K_p was inversely correlated to age and refraction. Measures proved accurate and reproducible. E is related to V_S, retinal traction and mechanical stimulation. Identified variables varied with age, refraction pathologic conditions.

1. Introduction

Human vitreous fluidics and the modifications secondary to aging and disease remain poorly understood due to the difficulty of *in vivo* measures and the intrinsic gel fragility that largely condition *in vitro* results (Lee et al., 1994a,b).

Many authors agree that vitreous dynamics plays a key role in the pathogenesis of prevalent vitreo-retinal diseases such as vitreous haemorrhage, peripheral retinal degeneration and tears, retinal detachment (RD) (Foster et al., 2010; Foster, 2011), myopia, diabetic retinopathy, macular edema (Schepens et al., 1984) and age-related macular degeneration (Krebs et al., 2007).

Quantitative measurement of vitreous motion has been attempted in the past: Walton et al. (2002) studied vitreous mobility by grading speckle density in ultrasound images and identified several kinematic parameters while Piccirelli et al. (2011) used MRI to assess vitreous velocity fields. Mathematical models have also been developed: David et al. (1998) studied the motion of a viscoelastic fluid in sphere performing small-amplitude oscillations and Repetto et al. (2010) proposed a model of vitreous motion in the presence of Posterior Vitreous Detachment (PVD), showing that vitreous oscillations can conceivably induce retinal tears.

Ocular Dynamic Ultrasound (ODU) allows *in vivo* imaging of vitreous motion, especially when syneresis, haeme or inflammation, enhance vitreous echogenity.

Robust Image Velocimetry (RIV) is an image analysis technique, derived from Particle Image Velocimetry (PIV) (Niu et al., 2010), which is widely used in fluid dynamics and provides statistical computation of motion patterns, also in presence of high levels of noise (Romano et al., 2010). Medical velocimetry based on ultrasound images has been recently developed (Kheradvar et al., 2010).

Purpose of present paper is to introduce Ultrasound Image Velocimetry (UIV) of the human eye using the RIV algorithm, test its repeatability and analyze the vitreous velocity fields generated by

* Corresponding author. Tel.: +39 348 2645034.
E-mail address: tommaso.rossi@usa.net (T. Rossi).

0014-4835/$ – see front matter © 2012 Elsevier Ltd. All rights reserved.
doi:10.1016/j.exer.2012.03.014

the saccade, in order to study vitreous motion *in vivo* and explore the potential for research and clinical application.

2. Materials and methods

2.1. Human eye ultrasonography technique

Twenty eyes of 20 patients with increased vitreous echogenity due to different conditions and followed by the Vitreoretinal Surgery Unit of the Eye Hospital of Rome, Italy, underwent ODU (Hi-Scan Digital Ultrasonograph – Optikon 2000 Inc., Rome, Italy). A 20 MHz B-Scan probe acquired 20 s sequence with an acquisition rate of 20 frames per second (fps). Temporal resolution was 0.05 s, probe lateral spatial resolution was 0.15 mm and axial resolution (antero-posterior) was 0.05 mm; US probe focal depth was 23 mm and depth of field (−6 dB) equal 6 mm. Movies were encoded into uncompressed avi format, to avoid loss of information.

ODU during ocular saccade was recorded after instructing patients to look all the way to their right and left upon request, while resting supine. A few seconds were allowed between consecutive saccades in order for the vitreous velocity to decay. Each patient underwent a training session of about 1 min before recording images. All scans were taken along the axial transverse plane to minimize vitreous motion away from the scan plane and patients underwent two sessions in randomized order by 2 experienced ophthalmologists.

Patients' exclusion criteria included the impossibility to fix and follow with the fellow eye and ocular muscle and/or neurologic deficiencies of any origin. Low quality images due to technical problems, vitreous insufficient echogenity, patients' compliance and overly motion artefacts were also discarded and patients removed from the study. Twelve eyes of 12 patients (Table 1) fulfilled inclusion criteria and were included.

2.2. Robust Image Velocimetry (RIV) from B-mode imaging

RIV extracts motion from B-mode movies by comparing corresponding regions of successive frames. The underlying assumption is that echogenic objects in the investigation regions translate, conserving their brightness during the time lapse between frames. As a consequence, the displacement minimizing the dissimilarity between the corresponding interrogation windows of two successive frames is assumed to be representative of the motion of the vitreous in that region. Compared to the classical PIV algorithm (Adrian, 2005), RIV uses a measure of dissimilarity which is statistically robust to outliers, thus resulting less affected by the presence of noise or artefacts in the images or by velocity differences within the interrogation windows (Falchi et al., 2006).

Table 1
Demographics and vitreous status of included patients. NA (=not applicable) refers to patients who had a previous pars plana vitrectomy and silicone oil tamponade removed. Vitreous chamber of such patients is therefore filled with aqueous and microscopic silicone oil droplets. RD = Retinal Detachment; VH = Vitreous Hemorrhage; PPV = Pars Plana Vitrectomy; PDMS = Poly-dimetylsiloxane; PDR = Proliferative Diabetic Retinopathy; TRD = Traction Retinal Detachment.

Patient	Sex	Age	Lens status	Refraction	Diagnosis	PVD
1, AI	M	67	Phakic	−15.50	Partial RD + VH	No
2, AP	M	56	Phakic	−22.00	Mild VH, highly myopic eye	Yes
3, BM	F	45	Phakic	+1.25	VH + choroidal detachment	No
4, CC	F	52	IOL	−4.25	Haeme in aqueous post PPV + partial RD (vitreous "skirt")	NA
5, DC	F	61	Phakic	Plano	VH	Yes
6, EC	M	44	Phakic	+0.50	VH	Yes
7, EMC	F	59	Phakic	−1.00	VH + partial RD	Yes
8, ED	M	62	Phakic	+0.50	VH + total RD	No
9, EM	F	74	Phakic	−8.00	Vitreitis	No
10, FB	F	57	IOL	−6.25	Total RD + PDMS emulsion post PDMS removal (s/p PPV)	NA
11, GA	F	55	Phakic	−11.00	VH + PDR + localized TRD	No
12, GS	M	48	Phakic	Plano	VH + partial RD	No

2.3. Velocity measures

The sclera–choroid–retina complex was manually traced for each patient, as the highly echogenic layer outlining the vitreous chamber and a reference point on the vitreo-retinal interface arbitrarily placed. Scleral angular velocity (V_S) was therefore defined as the ratio of the tangential velocity of this point to the radius of the vitreous chamber and expressed in rad/s. The geometric centre of the vitreous chamber was assumed as the rotation centre.

The vitreous chamber contour was recognized and velocity fields calculated for each couple of successive frames. The spatial average of the velocity on the plane of measure was then subtracted from the measured velocity. In this way it was possible to filter out the (small) solid body translation component of the velocity possibly arising from relative translational displacements between the ultrasound probe and position of the centre of rotation. We denote with V the vitreous velocity obtained this way and computed the squared velocity magnitude, $E = V^2$, which is, similarly to the velocity, a function of time and space and can be regarded as a measure of the kinetic energy per unit mass of the vitreous (except for a non relevant multiplicative constant). This yields information about the intensity of motion regardless of vector orientation. In order to analyze the time evolution of the overall energy of the vitreous, we indicated with E_S the spatial average of E, computed by the averaging all the velocities measured within the vitreous at the same time. As a consequence, E_S is only function of time. We also introduced the ratio between the peak value of E_S and the squared maximum scleral angular velocity during the same saccade, and indicated by K_p the average of that ratio over the saccades of each patient. Thus, K_p formalizes the relationship between scleral drive and vitreous response. Eight saccades per eye were considered: four on each side, alternated, starting and ending with zero scleral velocity ($V_S = 0$) in order to compensate for variations due to different or odd number of saccades.

In an attempt to characterize vitreous dynamics, the following measures were evaluated: vitreous motion onset time (T_O), calculated as the time interval between the peak scleral angular velocity and the following E_S peak and vitreous motion decay time (T_D), calculated as the time interval between the peak E_S and its decay to 1/10 of the original peak value (Fig. 1). Both T_O and T_D were averaged over 8 saccades of each eye.

In order to represent the spatial distribution of kinetic energy within the vitreous chamber, colour-coded maps of E_T, *i.e.* E averaged in time over 8 saccades, were also computed.

2.4. Statistical analysis

Scattergrams and Bland Altman diagrams (Bland and Altman, 1986, 1999) were plotted to test the repeatability and visualize the dispersion of V_S measures obtained by different operators. As suggested by Bland and Altman and following recommendations of the British Standards Institution, the coefficient of inter-operator reproducibility was defined as the standard deviation of differences between pairs of measurements obtained by the two operators divided by the average of the means of each pair. The lower values represented better repeatability. The limits of agreement were defined as 1.96 times the standard deviation of the differences among the measurements taken by the 2 operators, corresponding to the 97.5 percentile of the normal distribution.

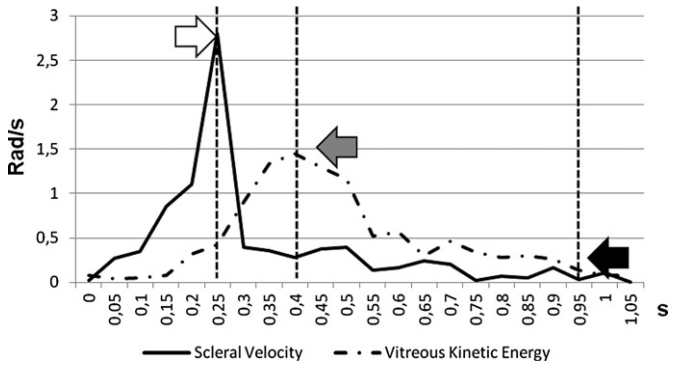

Fig. 1. Scleral velocity (continuous black line) versus vitreous kinetic energy (dash-dot line black line) plot spanning one single saccade. Arrows point peak scleral velocity (white), peak vitreous kinetic energy (grey) and 1/10 of peak vitreous kinetic energy (black). Vitreous motion onset time (T_O) is the time difference between grey and white arrow while vitreous motion decay time (T_D) is the time difference between the black and grey arrows time values.

Statistical analysis was based on univariate ANOVA, *t*-test and Pearson's *rho* correlation coefficient for continuous variables (V_S, E_S, K_p, T_O, T_D). Since T_O and T_D were calculated on video frames acquired at 20 fps, time was by definition estimated at discrete intervals of 0.05 s (1/20th of a second) and may be questioned as a continuous variable. For this reason T_O and T_D significance was also calculated by means of Kruskall–Wallis non-parametric test. Significance has been set at the 0.05 level in all cases.

3. Results

Results have been divided into 3 sections according to the rationale and progression of our study.

3.1. Measure consistency

Twelve eyes of 12 patients whose baseline data and demographics are reported in Table 1 met inclusion criteria. As an example of vector representation, vitreous velocity fields obtained at different times for patient #6 are shown in Fig. 2 and a real time velocity vector movie is enclosed (movie 1).

Supplementary video related to this article can be found at doi:10.1016/j.exer.2012.03.014.

Scleral velocity measures obtained by the 2 operators, both peak and average, did not differ statistically ($t = 1.032$; $p = 0.303$) and correlation between the operators was significant ($P = 0.592$; $p < 0.0001$) (Fig. 3). Peak V_S proved highly reproducible (Fig. 4), with only 5.8% falling out of the limits of agreement; inter-operator reproducibility coefficient was 0.043 and the agreement between the 2 operators, calculated as 1.96 × standard deviation of the mean difference was 0.63 rad/s. The mean V_S as measured by the 2 examiners combined, was 1.09 ± 0.32 rad/s and the mean difference was 0.048 ± 0.32 rad/s.

Vitreous velocity measures (reported as peak and average E_S) also did not differ significantly between operators and therefore none of the other variables reported in Table 2 did, since they all derive from V_S and E_S. Patients with varying clinical conditions, instead, returned different vitreous and scleral velocity values suggesting clinical condition more than operators influenced measures.

3.2. Vitreous velocity and fluidic parameters assessment

Table 3 reports the correlations between variables. Peak V_S positively correlated to vitreous peak kinetic energy (E_S) and vitreous velocity decay time. As a result, E_S was statistically correlated to vitreous velocity decay time also T_D.

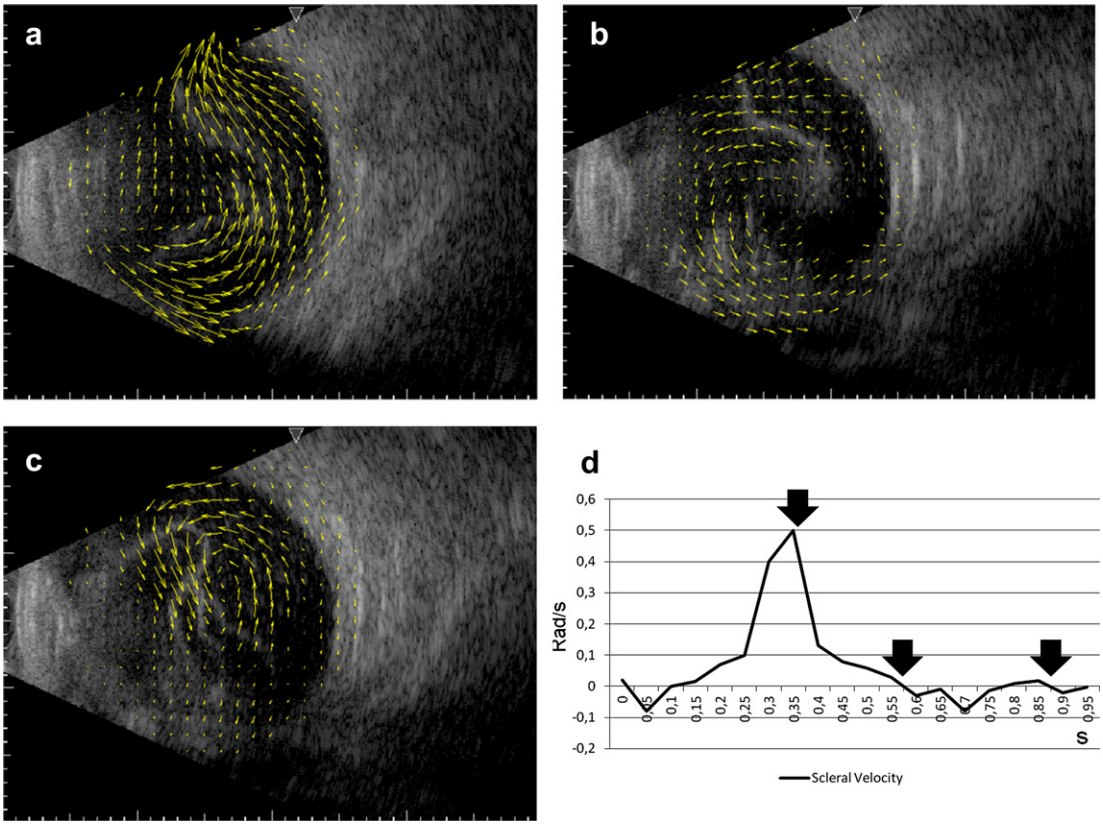

Fig. 2. Instantaneous velocity fields of patient #6 who developed a retinal detachment 1 month later (see Table 1). The three frames (a, b, c) are taken during the same saccade and d) plots scleral velocity versus time. The three arrows in plot d) represent the exact time frame for a), b), and c) respectively. Note the complexity of flow within the vitreous chamber.

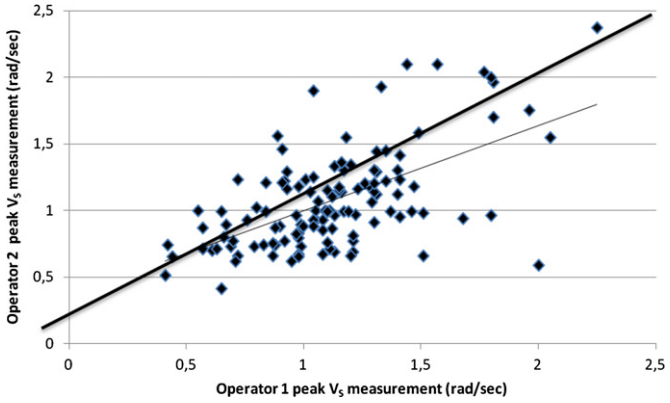

Fig. 3. Scattergam plot of V_S values for Operators 1 and 2. The solid thicker line indicates the quadrant bisector line ($y = x$), while the solid thinner line is the linear regression of observed values ($y = 0.639x + 0.355$).

Spatial colour maps of E_T, the time averaged E throughout the vitreous chamber of each patient, are reported in Fig. 5. Red and yellow identify higher E_T values.

3.3. Association of fluidics parameters to demographics and clinical conditions

The ratio of squared vitreous to scleral velocity (K_p; Table 3) inversely correlated to patients' age, suggesting that aging reduces energy transmission to the vitreous gel (Fig. 6). Also statistically significant was the inverse correlation between K_p and refraction, despite a limited sample. Highly myopic eyes, therefore, seem to translate less efficiently scleral velocity into vitreous kinetic energy (Fig. 7).

In a further effort to investigate whether a given clinical condition is associated to fluidic behaviour, so far not being able to infer diagnostic implications, we simply tabulated V_S, peak and average E_S, K_p, T_O and T_D against vitreous status and retinal detachment of our sample population (Table 4). The presence of PVD resulted in higher E_S, T_D and K_p while RD patients showed a significantly higher V_S and E_S.

4. Discussion

Although holding the promise of unravelling many of the vitreous–retina interaction secrets, vitreous dynamics remains largely speculative, due to the limited knowledge of its chemistry (Lee et al., 1994a,b), microscopic anatomy (Lee et al., 1992) and

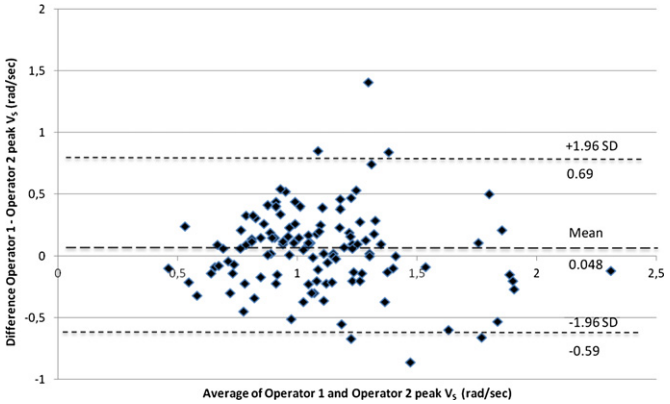

Fig. 4. Bland Altman graph. The mean of V_S measurements has been plot against their difference and limits of agreement set at ±1.96 SD.

Table 2
Calculated differences for measured variable among patients and operators. Significant values ($p < 0.05$) have been shaded in grey. (*Kruskall–Wallis non-parametric test for independents samples results are also reported for time variables, under the assumption that time measured in video frames is a non-continuous variable.). V_S = Velocity of the Sclera; E_S = Space averaged kinetic energy of the vitreous per unit mass; K_p = ratio of the peak value of E_S to peak value of the squared scleral angular velocity during the same saccade; T_O = vitreous motion onset time; T_D = vitreous motion decay time.

	Among patients	Among operators
Peak V_S	$F = 7.153$; $p < 0.0001$	$t = 1.032$; $p = 0.303$
Average V_S	$F = 18.486$; $p < 0.0001$	$t = 0.714$; $p = 0.398$
Peak E_S	$F = 15.132$; $p < 0.0001$	$F = 0.111$; $p = 0.740$
Average E_S	$F = 44.811$; $p < 0.0001$	$t = 0.109$; $p = 0.741$
K_p	$F = 5.440$; $p < 0.0001$	$F = 3.019$; $p = 0.085$
T_O	$F = 1.148$; $p = 0.334$	$F = 1.507$; $p = 0.222$
	$Chi^2 = 14{,}872$; $p = 0.188$*	$Chi^2 = 0.429$; $p = 0.512$*
T_D	$F = 28.142$; $p < 0.0001$	$F = 1.893$; $p = 0.172$
	$Chi^2 = 76{,}219$; $p < 0.0001$*	$Chi^2 = 0.000$; $p = 0.986$*

mechanical properties (Nickerson et al., 2008). Measuring ocular velocity fields *in vivo* represents an opportunity to understand vitreous motion, validate computational models (Buchsbaum et al., 1984) and possibly open new diagnostic perspectives.

Ultrasound velocimetry has been utilized in cardiology (Hong et al., 2008) but no ocular applications have been developed, to the best of our knowledge; we therefore meant to validate measurements consistency first.

V_S measures obtained by the two operators almost overlapped (Fig. 3) and over 94% of readings fell within the limits of agreement (Fig. 4), indicating good accuracy and repeatability. Peak V_S ranged between 1.32 and 3.65 rad/s (75–206 deg/s): slightly lower than reported in the literature (Robinson, 1964), probably due to the relatively low sampling frequency. Interestingly, operators did not bias either scleral or vitreous velocity that instead varied significantly among patients (Table 2).

The next step consisted in the assessment of vitreous motion through acquired data. The correlations we calculated appeared both physically meaningful and clinically suggestive (Table 3), indicating that higher scleral angular velocity (V_S) generates higher vitreous energy (E_S) and a longer decay time (T_D). Onset time (T_O), on the contrary, did not change significantly, nor did it correlate to any other variable (Table 3), as if vitreous response latency expressed invariant vitreous features. On the contrary, decay time (T_D) was significantly correlated to both V_S and E_S: reasonably enough, faster saccades generate higher E_S which, in turn, takes longer to damp.

When the ocular extrinsic muscles initiate the saccade, therefore, the vitreous lags a fraction of second behind the sclera and keeps moving after the sclera stops, pulling on the retina. In this scenario, energy transmission from the eyewall to the vitreous follows two basic mechanisms: where the vitreous is separated, viscosity determines a shear flow parallel to the retina. Conversely, where vitreo-retinal adhesions persist, a more complex mechanism mediated by extension of the adherence, vitreous viscoelasticity, mass and gel/sol ratio predominates.

The ratio K_p expresses the efficiency of kinetic energy transfer from the sclera to the vitreous, regardless to scleral velocity. K_p inversely correlated to age and refraction (Table 3), accounting for less efficient energy transmission in older and highly myopic patients (Figs. 6 and 7, respectively). Gel liquefaction and progressive separation of the posterior hyaloid from the retinal surface are clinically known to occur with age and increase with myopic refraction (Mitry et al., 2011). Although caution is warranted, given the uneven distribution of echogenity, the complex gel/sol mixture and the unpredictability of vitreo-retinal adhesion, we believe K_p ratio might help assess vitreous mechanical properties on an individual base.

Table 3
Pearsons' Correlation coefficient (Rho = R) and significance (p) of measured variables among patients. Correlations with $p < 0.05$ have been shaded in grey. V_S = velocity of the Sclera; E_S = space averaged kinetic energy of the vitreous per unit mass; K_p = ratio of the peak value of E_S (in time) to peak value of the squared scleral angular velocity during the same saccade; T_O = vitreous motion onset time; T_D = vitreous motion decay time.

	Age	Refraction	Peak V_S	Peak KE_V	K_p	VMOT	VMDT
Age	–	$R = -0.418$ $p = 0.177$	$R = 0.706$ $p = 0.10$	$R = 0.294$ $p = 0.354$	$R = -0.646$ $p = 0.023$	$R = 0.081$ $p = 0.803$	$R = 0.07$ $p = 0.983$
Refraction	$R = -0.418$ $p = 0.177$	–	$R = -0.526$ $p = 0.079$	$R = 0.196$ $p = 0.540$	$R = 0.799$ $P = 0.002$	$R = 0.387$ $p = 0.214$	$R = 0.088$ $p = 0.786$
Peak V_S	$R = 0.706$ $p = 0.10$	$R = -0.526$ $p = 0.079$	–	$R = 0.435$ $p < 0.0001$	$R = -0.558$; $p = -0.059$	$R = -0.083$ $p = 0.387$	$R = 0.210$ $p = 0.028$
Peak E_S	$R = 0.294$ $p = 0.354$	$R = 0.196$ $p = 0.540$	$R = 0.435$ $p < 0.0001$	–	$R = 0.435$ $p = 0.084$	$R = -0.012$ $p = 0.902$	$R = 0.422$ $p < 0.0001$
K_p	$R = -0.646$ $p = 0.023$	$R = 0.799$ $P = 0.002$	$R = -0.558$ $p = -0.059$	$R = 0.435$ $p = 0.084$	–	$R = 0.388$ $p = 0.212$	$R = -0.051$ $p = 0.876$
T_O	$R = 0.081$ $p = 0.803$	$R = 0.387$ $p = 0.214$	$R = -0.083$ $p = 0.387$	$R = -0.012$ $p = 0.902$	$R = 0.388$ $p = 0.212$	–	$R = -0.111$ $p = 0.247$
T_D	$R = 0.07$ $p = 0.983$	$R = 0.088$ $p = 0.786$	$R = 0.210$ $p = 0.028$	$R = 0.422$ $p < 0.0001$	$R = -0.051$ $p = 0.876$	$R = -0.111$ $p = 0.247$	–

Walton et al. (2002) studied vitreous mobility by grading ultrasound speckle density and concluded that angular velocity and vitreous motion overshoot correlated with age. They also reported higher speckle density and lower homogeneity in elderly patients. Piccirelli et al. (2011) used MRI to disclose correlation between saccadic phase angle and vitreous deformation that would in some cases point at a polyphasic vitreous structure. Indeed, the velocity fields we measured (Fig. 2), often showed E_T uneven distribution (Fig. 5) that suggests the presence of different phases (Mitry et al., 2010).

Mathematical models of vitreous motion induced by saccadic rotations have been developed: David et al. (1998) studied the motion of a viscoelastic fluid within an oscillating sphere and Meskauskas et al. (2011) extended the analysis finding that vitreous presents natural oscillation frequencies that saccades can possibly excite. Repetto et al. (2010) proposed a model of vitreous motion in the presence of PVD and showed that vitreous oscillations may cause retinal tears in the presence of strong vitreo-retinal adhesion.

The E_T maps we devised (Fig. 5), highlight kinetic energy spatial distribution, revealing unexpected details: high E_T values tend to localize either next to the equatorial retina (Fig. 5; patients AP, BM, CC, EM, FB, GA and GS) or the detached posterior hyaloid (Fig. 5; patients DC, EC and EMC). It seems that, provided posterior vitreo-retinal adhesion is present, E_T peaks closer to the retinal equatorial or pre-equatorial surface, while PVD tends to concentrate energy in the freely moving posterior hyaloid.

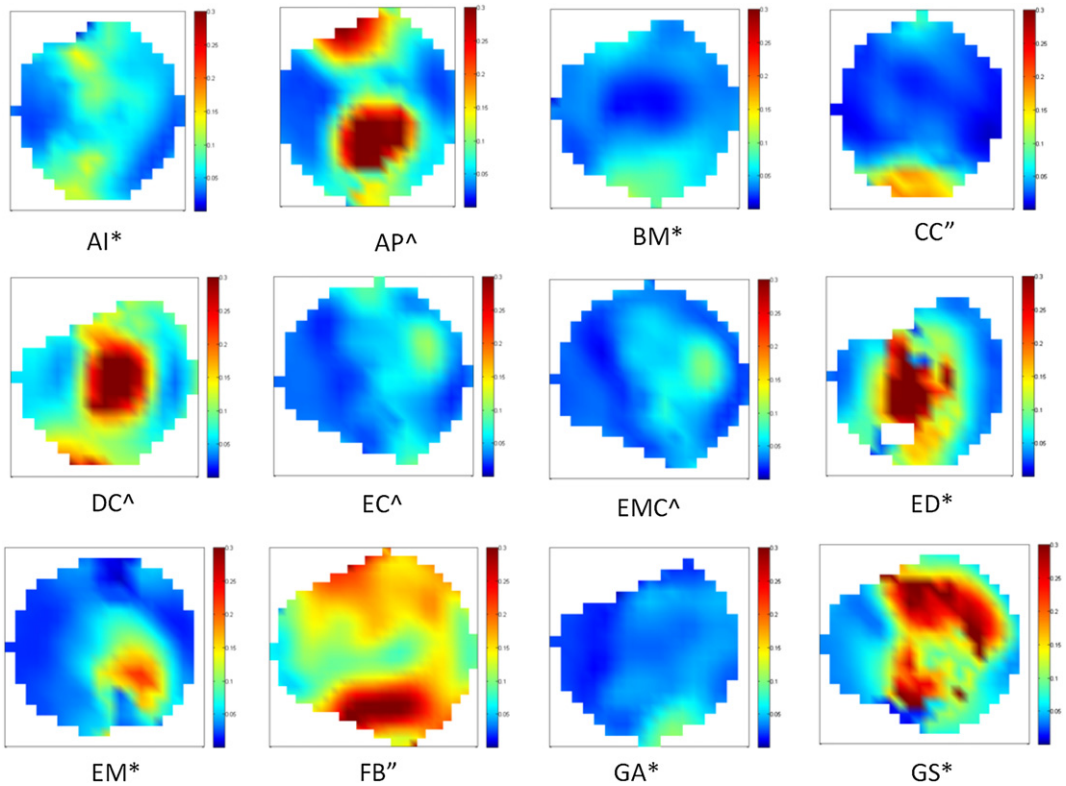

Fig. 5. Spatial maps of E_T as imaged by transverse axial B-Scan ultrasound. The ultrasound probe is located to the left of each map and therefore left-to-right is anterior to posterior. Colour scale is the same for all maps. See Table 1 for vitreous status details. (* = no previous Posterior Vitreous Detachment; ^ = previous Posterior Vitreous Detachment; “ = Aqueous filling the vitreous chamber post Pars Plana Vitrectomy and Silicone Oil Tamponade removal). (For interpretation of the references to colour in this figure legend, the reader is referred to the web version of this article.)

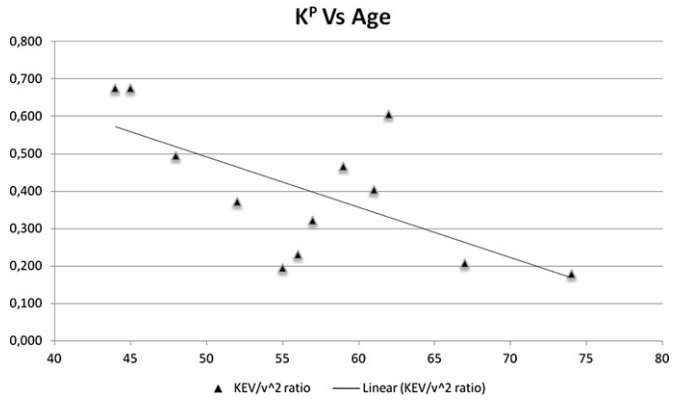

Fig. 6. K_p Scattergram plot as a function of age. Note than kinetic energy to squared scleral velocity ratio decreases as patients' age increases. In other words, as patients get older, less energy is transmitted from the sclera to the vitreous. The black line shows a linear regression function of experimental data.

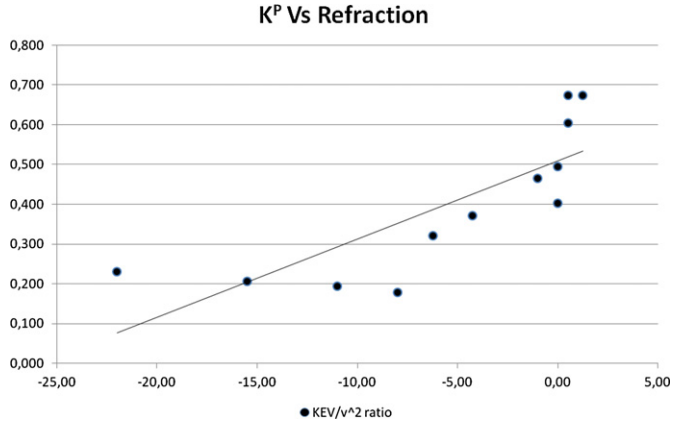

Fig. 7. K_p Scattergram plot as a function of refraction in spherical equivalent. To the left of the scattergram, highly myopic refractions seem to plateau on low K_p levels while the ration increases towards emmetropic refraction values becoming steeper for moderately hyperopic refractions. Continuous black line represents the linear regression of experimental data.

It is worth noting that in a perfect sphere filled with homogeneous viscous fluid, E_T should peak at the vitreo-retinal (fluid–solid) interface if shear stress is the main invoked mechanism. This is obviously not the case for most patients in our study (see Fig. 5) in which the highest E_T values are often reached within the core of the domain, implying the presence of significant heterogeneity and vitreo-retinal adhesion. Since no vitreous detachment ensues at the vitreous base, the angular velocity within this region is comparable to that of the sclera and is transferred to the posterior hyaloid with a sling mechanism instead of as shear stress through the neighbouring sclera. The elastic properties of the vitreous collagen fibrils probably amplify velocity and acceleration further, explaining the higher velocity of the posterior hyaloid.

When we looked at vitreous attachment status (Table 4), we found that, despite similar V_S, patients with no PVD had a lower E_S and much shorter T_D, suggesting that UIV can catch peculiar clinical features. This finding is consistent with what previously stated: the more posterior (and more diffuse) vitreous attachments remain (no PVD), the faster kinetic energy damps. The opposite holds for patients with complete PVD, in which similar V_S generates higher E_S that decays in longer times (Table 4). When incomplete PVD exists, the partially attached mass of gel retains kinetic energy for a longer time, stressing (i.e. exerting traction) residual retinal adhesions. It seems reasonable to assume that under these circumstances, one patient may be at higher risk for retinal breaks. As a matter of fact, one such patient (EC, Table 1) did later develop a retinal detachment.

Retinal status also related to vitreous dynamics (Table 4): RD eyes showed both a higher V_S and E_S, while vitreous motion onset and decay time where comparable. We are unable to offer an explanation since ours is only a feasibility study; however, results suggest that greater V_S may predispose to RD, generating higher E_S.

Present study suffers from many pitfalls, some related to ultrasound image acquisition and UIV analysis itself. Vitreous echogenity, in fact, can vary according to numerous conditions: there can be loss of signal due to speckles falling off the scan plane and discriminate between a region with lack of echogenity and a region where the vitreous does not move is impossible. Ultrasound probe sensitivity and the ideal focal plane and depth of field should also be optimized according to the specific task of getting signal from the vitreous chamber. Future test will include determination of ideal ultrasound frequency and focal plane that may differ from those routinely used for diagnostic ultrasound.

We decided to test UIV on pathologic vitreous to take advantage of the highest possible echogenity, improve signal to noise ratio and obtain a thorough representation of vitreous motion. Once UIV feasibility is ascertained, future extensive testing of physiologic vitreous will be necessary to evaluate diagnostic and prognostic capability; this will most likely require machines that are more sensitive and a higher frame per second acquisition rate.

From the clinical point of view, it should be emphasized that no conclusion can be drawn since the study merely aimed at determining feasibility and measure reproducibility. Saccade speed variability could also be regarded as a bias source although K_p ratio was introduced exactly to overcome this and adimensionally assess vitreous motion per scleral velocity unit.

Despite the many difficulties of entering a new field, we believe the application of UIV to ocular ultrasound is a promising research

Table 4
Calculated differences for measured variable as a function of vitreous and retinal status. Significant values ($p < 0.05$) have been shaded in grey. RD = Retinal Detachment; PVD = Posterior Vitreous Detachment; V_S = velocity of the sclera; E_S = kinetic energy of the vitreous per unit mass; K_p = ratio of the peak value of E_S to peak value of the squared scleral angular velocity during the same saccade; T_O = vitreous motion onset time; T_D = vitreous motion decay time.

	PVD				RD		
	No	Yes	Post PPV	p	No	Yes	P
Peak V_S [rad/s]	1.16 ± 0.44	1.10 ± 0.33	1.23 ± 0.49	$F = 0.526$; $p = 0.592$	1.08 ± 0.31	1.24 ± 0.50	$F = 4.051$; $p = 0.047$
Average V_S [rad/s]	0.17 ± 0.28	0.16 ± 0.25	0.17 ± 0.25	$F = 1.019$; $p = 0.361$	0.15 ± 0.25	0.18 ± 0.29	$F = 23.797$; $p < 0.0001$
Peak E_S [m^2/s^2]	0.48 ± 0.25	0.64 ± 0.14	0.58 ± 0.33	$F = 4.375$; $p = 0.015$	0.45 ± 0.41	0.64 ± 0.25	$F = 17.03$; $p < 0.001$
Average E_S [m^2/s^2]	0.06 ± 0.13	0.08 ± 0.15	0.08 ± 0.17	$F = 19.375$; $p < 0.001$	0.06 ± 0.12	0.08 ± 0.16	$F = 43.956$; $p < 0.0001$
K_p [m^2]	0.34 ± 0.35	0.36 ± 0.21	0.51 ± 0.14	$F = 0.728$; $p = 0.050$	0.39 ± 0.23	0.41 ± 0.14	$F = 0.027$; $p = 0.874$
T_O [s]	0.10 ± 0.24	0.07 ± 0.03	0.08 ± 0.03	$F = 0.271$; $p = 0.763$	0.07 ± 0.06	0.11 ± 0.27	$F = 1.331$; $p = 0.251$
T_D [s]	0.17 ± 0.08	0.29 ± 0.01	0.26 ± 0.08	$F = 13.295$; $p < 0.0001$	0.21 ± 0.13	0.23 ± 0.09	$F = 0.743$; $p = 0.391$

and possibly diagnostic tool. Technical refinement and standardization will allow the definition of vitreous dynamics normative data and allow the detection of abnormalities that may predispose to retinal traction, tears and RD and, hopefully, assist the ophthalmologist determining the individual risk for retinal accidents.

Financial disclosure

Giacomo Pasqualitto is an employee of Optikon 2000 Inc.; none of the other authors has any financial interest in the subject matter and no financial support is involved in the study.

References

Adrian, R., 2005. Twenty years of particle image velocimetry. Exp. Fluids 39, 159–169.
Bland, J.M., Altman, D.G., 1986. Statistical method for assessing agreement between two methods of clinical measurement. Lancet 1, 307–310.
Bland, J.M., Altman, D.G., 1999. Measuring agreement in method comparison studies. Stat. Methods Med. Res. 8, 135–160.
Buchsbaum, G., Sternklar, M., Litt, M., Grunwald, J.E., Riva, C.E., 1984. Dynamics of an oscillating viscoelastic sphere: a model of the vitreous humor of the eye. Biorheology 21 (1–2), 285–296.
David, T., Smye, S., Dabbs, T., James, T., 1998. A model for the fluid motion of vitreous humour of the human eye during saccadic movement. Phys. Med. Biol. 43, 1385–1399.
Falchi, M., Querzoli, G., Romano, G.P., 2006. Robust evaluation of the dissimilarity between interrogation windows in image velocimetry. Exp. Fluids 41 (2), 279–293.
Foster, W.J., Dowla, N., Joshi, S.Y., Nikolaou, M., 2010. Graefes Arch. Clin. Exp. Ophthalmol. 248 (1), 31–36.
Foster, W.J., 2011. Bilateral patching in retinal detachment: fluid mechanics and retinal “settling”. Invest. Ophthalmol. Vis. Sci. 20 52 (8), 5437–5440.
Hong, G.R., Pedrizzetti, G., Tonti, G., Li, P., Wei, Z., Kim, J.K., Baweja, A., Liu, S., Chung, N., Houle, H., Narula, J., Vannan, M.A., 2008. Characterization and quantification of vortex flow in the human left ventricle by contrast echocardiography using vector particle image velocimetry. JACC Cardiovasc. Imaging 1 (6), 705–717. Epub 2008 Nov 18.
Kheradvar, A., Houle, H., Pedrizzetti, G., Tonti, G., Belcik, T., Ashraf, M., Gharib, M., Sahn, D., 2010. Echocardiographic particle image velocimetry: a novel technique for quantification of left ventricular blood vorticity pattern. J. Am. Soc. Echocardiogr. 23, 86–94.
Krebs, I., Brannath, W., Glittenberg, C., Zeiler, F., Sebag, J., Binder, S., 2007. Posterior vitreomacular adhesion: a potential risk factor for exudative age-related macular degeneration? Am. J. Ophthalmol. 144 (5), 741–746 Epub 2007 Sep 20.
Lee, B., Litt, M., Buchsbaum, G., 1992. Rheology of the vitreous body. Part I: Viscoelasticity of human vitreous. Biorheology 29 (5–6), 521–533.
Lee, B., Litt, M., Buchsbaum, G., 1994a. Rheology of the vitreous body: part 2. Viscoelasticity of bovine and porcine vitreous. Rheology 31 (4), 327–338.
Lee, B., Litt, M., Buchsbaum, G., 1994b. Rheology of the vitreous body: part 3. Concentration of electrolytes, collagen and hyaluronic acid. Biorheology 31 (4), 339–351.
Meskauskas, J., Repetto, R., Siggers, J.H., 2011. Oscillatory motion of a viscoelastic fluid within a spherical cavity. J. Fluid Mech. 685, 1–22.
Mitry, D., Fleck, B.W., Wright, A.F., Campbell, H., Charteris, D.G., 2010. Pathogenesis of rhegmatogenous retinal detachment: predisposing anatomy and cell biology. Retina 30 (10), 1561–1572.
Mitry, D., Singh, J., Yorston, D., Siddiqui, M.A., Wright, A., Fleck, B.W., Campbell, H., Charteris, D.G., 2011. The predisposing pathology and clinical characteristics in the Scottish retinal detachment study. Ophthalmology 118 (7), 1429–1434. Epub 2011 May 10.
Nickerson, C.S., Park, J., Kornfield, J.A., Karageozian, H., 2008. Rheological properties of the vitreous and the role of hyaluronic acid. J. Biomech. 41, 1840–1846.
Niu, L., Qian, M., Wan, K., Yu, W., Jin, Q., Ling, T., Gao, S., Zheng, H., 2010. Ultrasonic particle image velocimetry for improved flow gradient imaging: algorithms, methodology and validation. Phys. Med. Biol. 7 55 (7), 2103–2120. Epub 2010 Mar 19.
Piccirelli, M., Bergamin, O., Landau, K., Boesiger, P., Luechinger, R., 2011. Vitreous deformation during eye movement. NMR Biomed. 25, 59–66.
Repetto, R., Tatone, A., Testa, A., Colangeli, E., 2010. Traction on the retina induced by saccadic eye movements in the presence of posterior vitreous detachment. Biomech. Model. Mechanobiol. 10, 191–202.
Robinson, D.A., 1964. The mechanics of human saccadic eye movements. J. Physiol. 174, 245–264.
Romano, G.P., Querzoli, G., Falchi, M., 2010. Investigation of vortex dynamics downstream of moving leaflets using robust image velocimetry. Exp. Fluids 4, 827–838.
Schepens, C.L., Avila, M.P., Jalkh, A.E., Trempe, C.L., 1984. Role of the vitreous in cystoids macular edema. Surv. Ophthalmol. 28, 499–504.
Walton, K.A., Meyer, C.H., Harkrider, C.J., Cox, T.A., Toth, C.A., 2002. Age-related changes in vitreous mobility as measured by video B scan ultrasound. Exp. Eye Res. 74, 173–180.